Fermi National Accelerator Laboratory

FERMILAB-TM-1930
D0

Improvement to the D0 Luminosity Monitor Constant

J. Bantly et al.
For the D0 Luminosity Working Group

Fermi National Accelerator Laboratory
P.O. Box 500, Batavia, Illinois 60510

March 1996

Operated by Universities Research Association Inc. under Contract No. DE-AC02-76CHO3000 with the United States Department of Energy

Disclaimer

Fermilab-TM-1930
DØ Note 2544
Dec. 29, 1995

Improvement to the DØ Luminosity Monitor Constant

J.Bantly, A.Brandt, R.Partridge,
J.Perkins, D.Puseljic

for the DØ Luminosity Working Group

Abstract

The DØ experiment has previously calculated its luminosity using the visible cross section (luminosity monitor constant) for its Level Ø trigger, $\sigma_{\mathrm{L}\emptyset} = 48.2$ mb, based on the world average $\overline{p}p$ inelastic cross sections at $\sqrt{s} = 1.8$ TeV. The error on luminosity had been set at 12%. Recent studies using the MBR and DTUJET Monte Carlo event generators and unbiased DØ data samples have resulted in a more precise determination of the DØ luminosity monitor constant. The result, $\sigma_{\mathrm{L}\emptyset} = 46.7 \pm 2.5$ mb, lowers the central value by 3.1% and reduces the error to 5.4%.

1 Introduction

The DØ experiment [1] decided to adopt the 'world average' values for the total, elastic, and single diffractive cross sections in the summer of 1994 [2]. The decision to adopt a 'world average' at $\sqrt{s} = 1.8$ TeV led to a recalculation of the DØ luminosity monitor constant, $\sigma_{\mathrm{L}\emptyset}$. However, at that time, the error on $\sigma_{\mathrm{L}\emptyset}$ was left at 12% due to uncertainties about correlated errors and input parameters. The original study used only MBR with a much simpler detector simulation and was completed before the DØ experiment took beam data. Since then, studies have been made using the MBR (Appendix B of Ref. [3]) and DTUJET-93 [4] Monte Carlo event generators. The generators

produced single diffractive, double diffractive, and hard core inelastic scattering event samples which were passed through the DØ version of GEANT [5] to simulate particle showering and detector effects. These samples were used to determine the acceptances of the Level Ø (LØ) trigger system [6] for the three inelastic processes. The overall LØ efficiency was determined from unbiased DØ data samples. The input data and the recalculation for $\sigma_{\mathrm{L}\emptyset}$ are described below.

2 The Level Ø Trigger

The LØ trigger is a fast triggering system for the DØ detector. Details of the LØ detector and its electronics are available in the LØ trigger reference [6]. For each beam crossing (occurring every 3.5μs), the LØ trigger indicates which of them contain non-diffractive inelastic collisions and monitors the instantaneous luminosity. The LØ detector is comprised of two hodoscope scintillator arrays located on the inside faces of the DØ detector's two end calorimeters, 140 cm from the center of the detector. Each array partially covers a region in pseudorapidity of $1.9 < |\eta| < 4.3$, with nearly complete coverage over $2.2 < |\eta| < 3.9$. The pseudorapidity coverage is motivated by the requirement that a coincidence of both LØ arrays be $\geq 99\%$ efficient in detecting non-diffractive inelastic collisions.

Analog sums are formed of the 20 LØ counters closest to the beam pipe for each of the north and south LØ arrays. These two analog sums are passed through constant fraction discriminators and fed into the FASTZ electronics module. The module uses the arrival time difference between the two sums to select events with $|z| < 96$ cm (good FASTZ), where z is the position along the beam axis measured from the center of the DØ detector. The discriminator outputs of the two analog sum signals are also fed into Flash ADCs from which the arrival times can be obtained with an accuracy of approximately 1 nsec. The arrival times are used to determine if there were hits seen in both LØ counters in time with the beam crossing. The FASTZ trigger is used to count beam crossings with inelastic collisions for the luminosity measurements made at DØ. In addition, the LØ trigger provides measurements of the interaction position along the beam axis for use in early trigger decisions and measurements of beam halo.

3 Instantaneous Luminosity based on LØ Scaler Rates

The instantaneous luminosity $\mathcal{L}$ is related to the counting rate $R_{\mathrm{L}\emptyset}$ in the LØ counters by:

$$\mathcal{L} = \frac{R_{\mathrm{L}\emptyset}}{\sigma_{\mathrm{L}\emptyset}} \tag{1}$$

where $\sigma_{\mathrm{L}\emptyset}$ is the cross section subtended by these counters. The counting rate (and, thus, the instantaneous luminosity $\mathcal{L}$) is measured for each of the six bunch crossings.

This is strictly true only if the instantaneous luminosity is low enough that the counting rate corresponds to the interaction rate. As the luminosity increases there is the possibility for having multiple interactions in a single crossing. For this case, the counting rate is less than the interaction rate since multiple interactions get counted only once.

The multiple interaction correction may be calculated based on Poisson statistics. The average number of interactions per crossing, $\bar{n}$, is given by:

$$\bar{n} = \mathcal{L}\ \tau\ \sigma_{\mathrm{L}\emptyset} \tag{2}$$

where τ is the crossing time ($\tau = 3.5\ \mu$s). The multiple interaction correction factor is then:

$$\frac{\mathcal{L}}{\mathcal{L}_{\mathrm{meas}}} = \frac{\bar{n}}{1 - e^{-\bar{n}}} = \frac{-\ln(1 - \mathcal{L}_{\mathrm{meas}}\ \tau\ \sigma_{\mathrm{L}\emptyset})}{\mathcal{L}_{\mathrm{meas}}\ \tau\ \sigma_{\mathrm{L}\emptyset}} \tag{3}$$

4 The LØ Trigger Efficiency

The LØ trigger efficiency was determined by using samples of DØ data collected while triggering on random beam crossings (zero bias). These unbiased data samples are collected by triggering the DØ data acquisition system [1] solely on the crossing time of the $\overline{p}p$ beams at the DØ collision region and not on the presence of an interaction.

We measure the LØ pedestals using those zero bias data events with no LØ hits in-time with the beam crossing. The distributions of charge from the analog sums are shown in Figure 1. The peaks show the locations of the pedestals of the two arrays. The charge distribution for the north (south)

LØ array when an in-time hit is seen in the south (north) array is shown in Figure 2(a) (2(b)). One should note that Figures 2(a) and 2(b) show only the threshold region, with most events overflowing the plot. To eliminate the effects of satellite-satellite collisions and beam halo, we require either a good FASTZ and in-time hits on both ends or a bad FASTZ and no hit close to being in-time. This cut also excludes events with $|z| > 96$ cm, which is an inefficiency common for both the luminosity counting and physics triggers; thus having no effect on cross section measurements. Figures 2(a) and 2(b) show a pedestal peak due to crossings where no particles hit the LØ array on top of a smooth charge distribution from events where both arrays are hit. The charge distributions for events with a good FASTZ are shown by the dashed lines.

To estimate the LØ efficiency, we subtract off the pedestal peak in Figure 2, assuming it has the same shape as in Figure 1, with a normalization determined using the four bins in the pedestal peak. The major uncertainty in this subtraction is the number of events that have a particle hitting the LØ array with a charge in the normalization region. We assume the charge distribution for these events is flat with a magnitude obtained by averaging the bins just above the pedestal peak bins and assign a 100% error to the magnitude obtained. After subtracting the pedestal peak, we determine the LØ efficiency for each end from the fraction of events that have a good FASTZ. The events having a good FASTZ are shown as the dashed distributions in Figures 2(a) and 2(b). The final LØ efficiency is obtained by taking the product of the efficiencies of the north and south arrays. Poisson statistics is used to correct for the effects of multiple interactions. The results are shown in Table 1.

5 Inelastic Scattering Cross Sections

The total, elastic and single diffractive cross sections from E710 [8] and CDF [3] [9] [10] are assembled in Table 2. The weighted means and errors for the combined cross sections, used to determine LØ, are given in Table 3; further details can be found in Ref [2]. Because of the large differences between the two experiments, the error on the inelastic cross section, $\sigma_{inelastic}$, has been scaled by χ taken from the χ^2 of the probability that the two values, within quoted errors, are the same. In addition, the E710 single arm (SA)

$\epsilon_{L\emptyset}^{North}$	$0.988 \pm 0.006 \pm 0.004$
$\epsilon_{L\emptyset}^{South}$	$0.982 \pm 0.005 \pm 0.004$
$\epsilon_{L\emptyset}^{Total}$	$0.970 \pm 0.007 \pm 0.008$
LØ FASTZ Luminosity	$5.32 \times 10^{30}/(cm^2 sec)$
Corrected Luminosity	$5.59 \times 10^{30}/(cm^2 sec)$
Corrected $\epsilon_{L\emptyset}$	0.95 ± 0.02

Table 1: LØ efficiency.

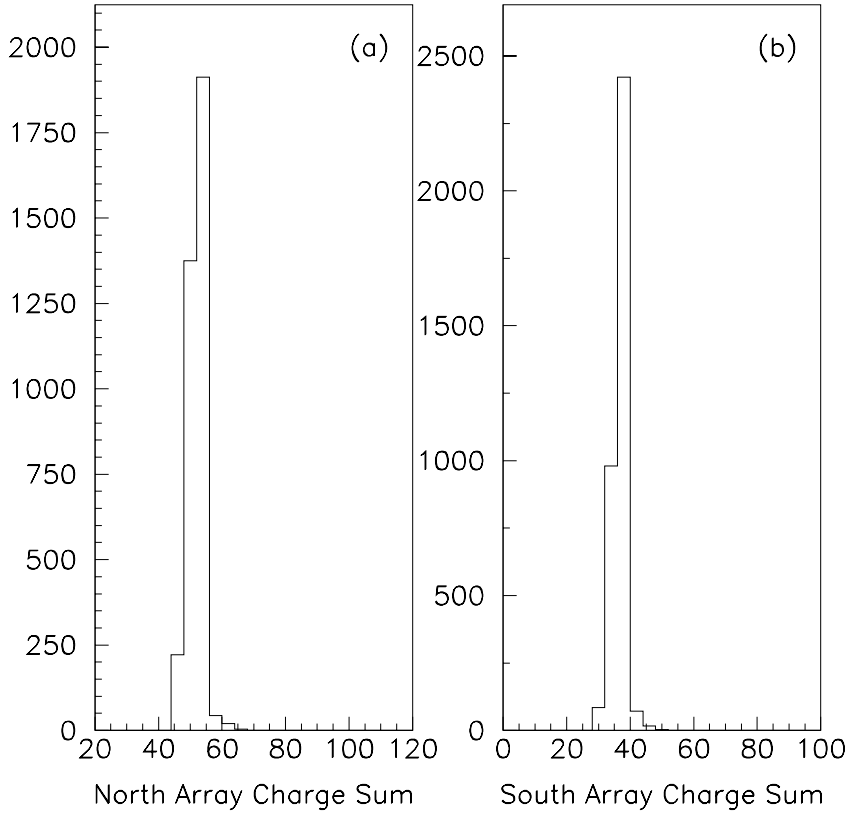

Figure 1: The distribution of charge from the north (south) LØ analog sums in ADC units when no in-time hits are present.

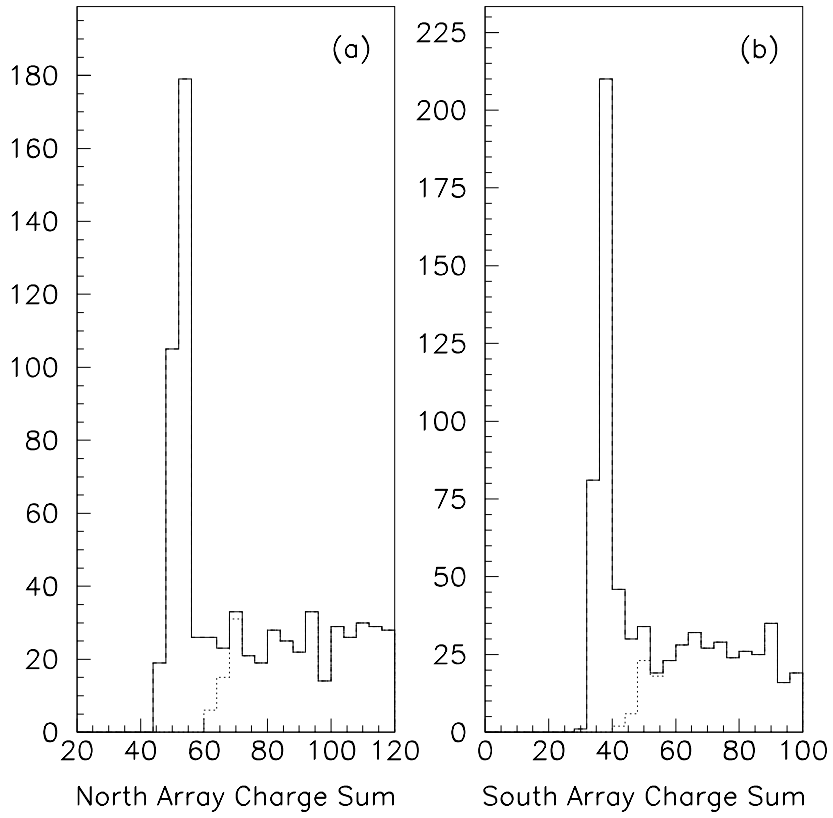

Figure 2: The distribution of charge from the north (south) LØ analog sums in ADC units when there is an in-time hit on the south (north) LØ array. The dashed curves show the distribution of those crossings that also fired the LØ FASTZ trigger.

	Mean	Error
CDF Elastic Cross Section	19.70 mb	0.85 mb
CDF Inelastic Cross Section	60.33 mb	1.4 mb
CDF SD Cross Section	9.46 mb	0.44 mb
E710 Elastic Cross Section	16.6 mb	1.6 mb
E710 Inelastic Cross Section	55.5 mb	2.2 mb
E710 SD (SA) Cross Section	11.7 mb	2.3 mb

Table 2: CDF and E710 cross sections.

	Mean	Error
Average Inelastic Cross Section	58.9 mb	1.2 mb
Average SD Cross Section	9.5 mb	0.4 mb
Inelastic Cross Section χ^2	3.43	
SD Cross Section χ^2	0.92	
Inelastic Error Scale Factor χ	1.85	
SD Error Scale Factor	1.0	
Inelastic Cross Section ($\sigma_{inelastic}$)	58.94 mb	2.19 mb
SD Cross Section ($\sigma_{\rm SD}$)	9.54 mb	0.43 mb

Table 3: 'World Average' cross sections based on CDF and E710 results.

cross section was used for the E710 single diffractive result as it more closely represents the physics signal seen by the LØ trigger than the more recent E710 single diffractive result [11].

The double diffractive cross section, $\sigma_{\rm DD}$, is not a direct measurement but is calculated using the elastic and single diffractive cross sections, $\sigma_{\rm EL}$ and $\sigma_{\rm SD}$ respectively. The calculation uses factorization (see Figure 3) to approximate the equivalence of the ratio:

$$\frac{\sigma_{\rm DD}}{\sigma_{\rm SD}} \approx \frac{\sigma_{\rm SD}}{\sigma_{\rm EL}} \tag{4}$$

Since the single diffractive cross sections from Table 2 include either particle

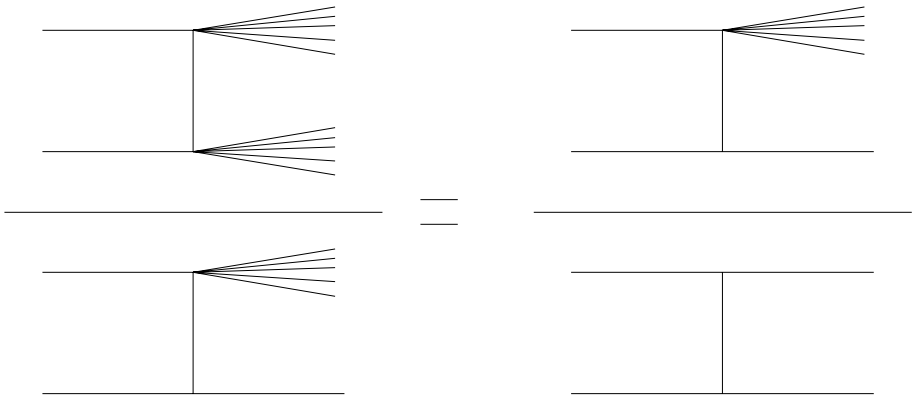

Figure 3: Factorization to approximate the double diffractive cross section, $\sigma_{\rm DD}$.

diffracting, $\sigma_{\rm SD}$ in Equation 4 is replaced by $\sigma_{\rm SD}/2$. A 10% systematic error is applied to this factorization method [12]. This makes the double diffractive cross section

$$\sigma_{\rm DD} \approx \frac{\sigma_{\rm SD}^2}{4\sigma_{\rm EL}} \tag{5}$$

The double diffractive cross section is calculated for both the CDF and E710 values of the single diffractive and elastic cross sections. A 'world average' weighted mean and error is calculated and the results are given in Table 4. This measurement is also in good agreement with the $\sigma_{\rm DD}$= 1.3 mb obtained by Goulianos [12].

The hard core component of the inelastic cross section is simply the inelastic cross section with the single and double diffractive components subtracted off.

$$\sigma_{\rm HC} = \sigma_{\rm Inelastic} - \sigma_{\rm SD} - \sigma_{\rm DD} \tag{6}$$

The result is $\sigma_{\rm HC}$= 48.25$\pm$2.23 mb.

The 'world average' cross sections based on the CDF and E710 numbers are used in the final determination of $\sigma_{\rm L\emptyset}$ in Section 7.

	Mean	Error
CDF Elastic Cross Section	19.70 mb	0.85 mb
CDF SD Cross Section	9.46 mb	0.44 mb
CDF DD Cross Section	1.14 mb	0.12 mb
E710 Elastic Cross Section	16.6 mb	1.6 mb
E710 SD (SA) Cross Section	11.7 mb	2.3 mb
E710 DD Cross Section	2.1 mb	0.8 mb
Weighted Mean $\sigma_{\rm DD}$	1.15 mb	0.12 mb
Double Diffractive χ^2	1.207	
DD Error Scale Factor	1.0	
Factorization Error		0.115 mb
World Average $\sigma_{\rm DD}$	1.15 mb	0.17 mb

Table 4: Double diffractive cross section.

6 Level Ø Acceptances for Inelastic Scattering Processes

We use two independent inelastic Monte Carlo generators to study the LØ acceptance. The MBR Monte Carlo is based on CDF multiplicity studies and the DTUJET Monte Carlo uses the Dual Parton Model to simulate the underlying physics. Each Monte Carlo has separate switches to allow the generation of single diffractive, double diffractive, and hard core (inelastic non-diffractive) events separately. Six 1000-event samples were generated, corresponding to the different combinations of generator and process. The samples were passed through the full DØ GEANT simulation and reconstructed with standard offline code. A slight modification was made to the detector simulation to correct for a pair of beam pipe bellows that were missing from the original simulation. For each sample, we calculate the fraction of events that would fire the LØ FASTZ trigger, which is determined by having at least one particle pass through each of the north and south arrays. The final columns in Tables 5 and 6 show these LØ acceptances for DTUJET and MBR respectively. The two Monte Carlos give similar but not identical results, with the single diffractive acceptance ranging from 10 to

20%, the double diffractive acceptance 69 to 75%, and the hard core inelastic acceptance between 95 to 99%.

The tables also show cross–checks with data where possible. Cross checks were made using a zero bias sample (only a beam crossing is required) obtained at an instantaneous luminosity of $1.5 \times 10^{30} cm^{-2} s^{-1}$. At this luminosity, crossings with at least one inelastic collision are predominately single interaction crossings (>98 %). The data are compared to the single diffractive Monte Carlos for the case where only one LØ array is hit, since the data are dominated by single diffractive exchange for this topology. The mean number of LØ counters hit is seen to be slightly lower than, but in reasonable agreement with, the data. Figure 4 shows the distribution of the number of counters hit in the north array when there are no hits in the south array. The solid line is the data, the dashed line is from the DTUJET single diffractive sample and the dotted curve is the MBR sample. Figure 5 shows the distribution of energy in the north DØ end calorimeter ($\eta > 1.3$). The three distributions are very similar. The mean energies are listed in Tables 5 and 6.

Demanding that both LØ arrays be hit provides a data sample that can be compared with the hard core inelastic Monte Carlo samples. The mean number of counters hit is seen to be a bit low as was the case in the single diffractive samples. This can be seen also in Figure 6, where the curves are the same as in Figure 4 except the hard core samples are used. The average end calorimeter energy is in reasonable agreement between the data and the Monte Carlo samples and is shown in Figure 7. The slightly lower average multiplicity is expected if the modification to include the beam pipe bellows did not put enough material in that location. Event samples generated with and without this modification showed the extra material caused an increase in multiplicity of LØ counters hit, but almost no change in the total energy deposited in the end calorimeters. An estimate of the extra material needed to match the multiplicity distributions is approximately half a radiation length.

The average acceptance values are given in Table 7, where the systematic error is one-half the difference between the two generators.

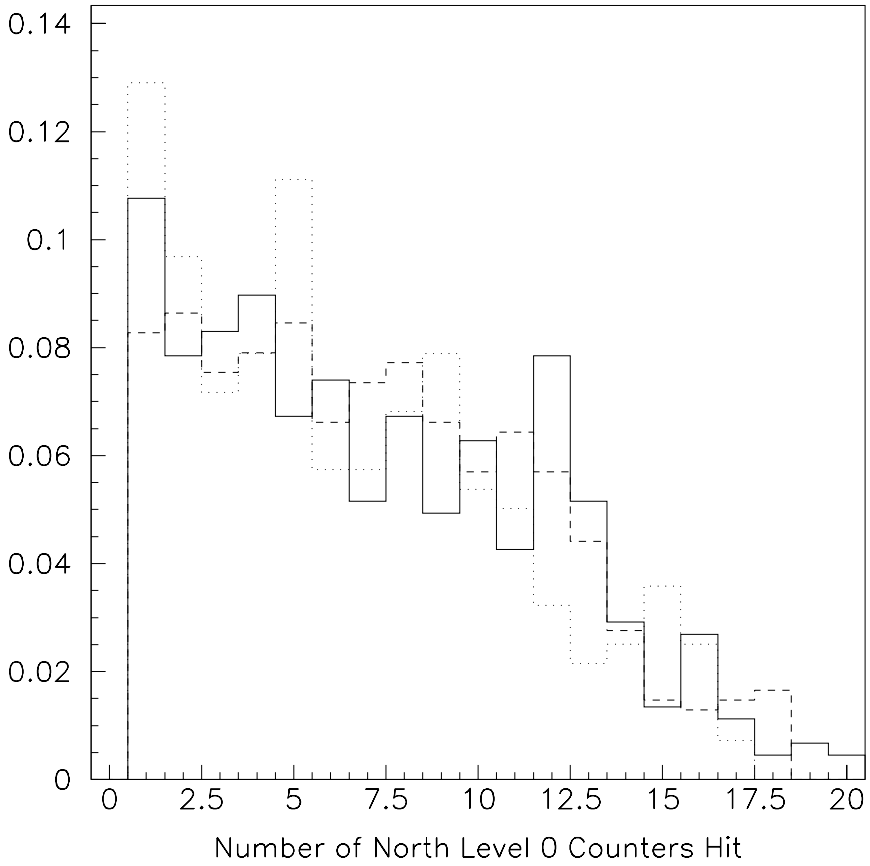

Figure 4: The distribution of the number of counters hit in the north array when there are no hits in the south array. The solid line is the data, the dashed line is from the DTUJET single diffractive sample and the dotted curve is the MBR sample.

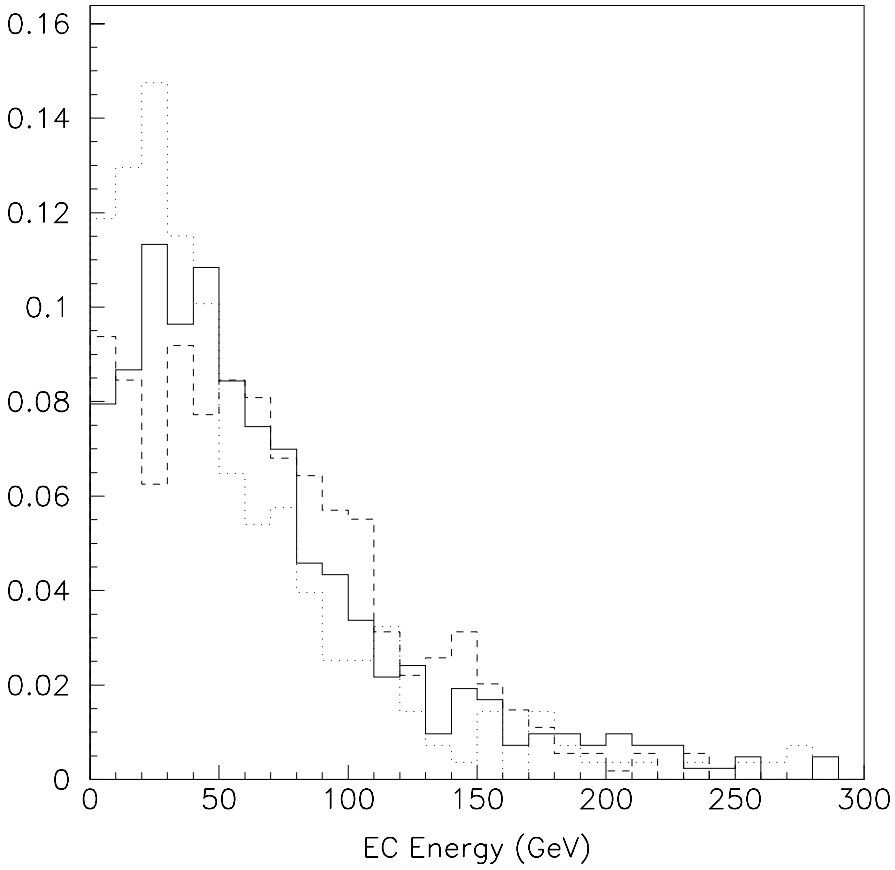

Figure 5: The distribution of energy deposited in the north DØ end cap calorimeter ($\eta > 1.3$) when there are no hits in the south LØ array. The solid line is the data, the dashed line is from the DTUJET single diffractive sample and the dotted curve is the MBR sample.

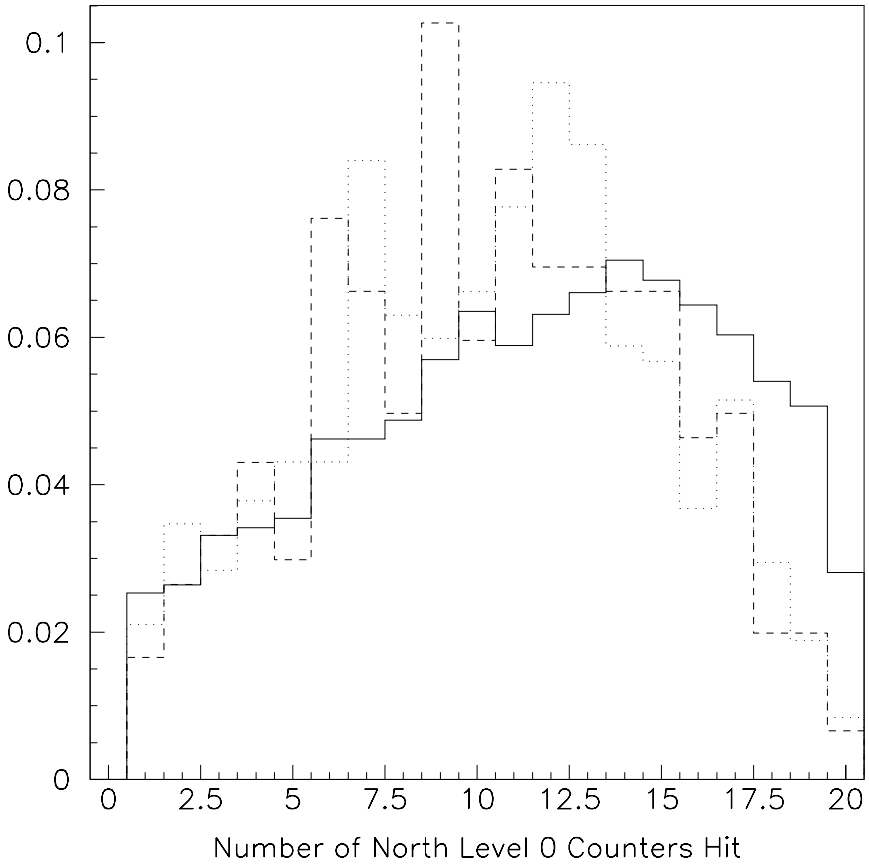

Figure 6: The distribution of the number of counters hit in the north array when there are hits in the LØ arrays. The solid line is the data, the dashed line is from the DTUJET hard core inelastic sample and the dotted curve is the MBR sample.

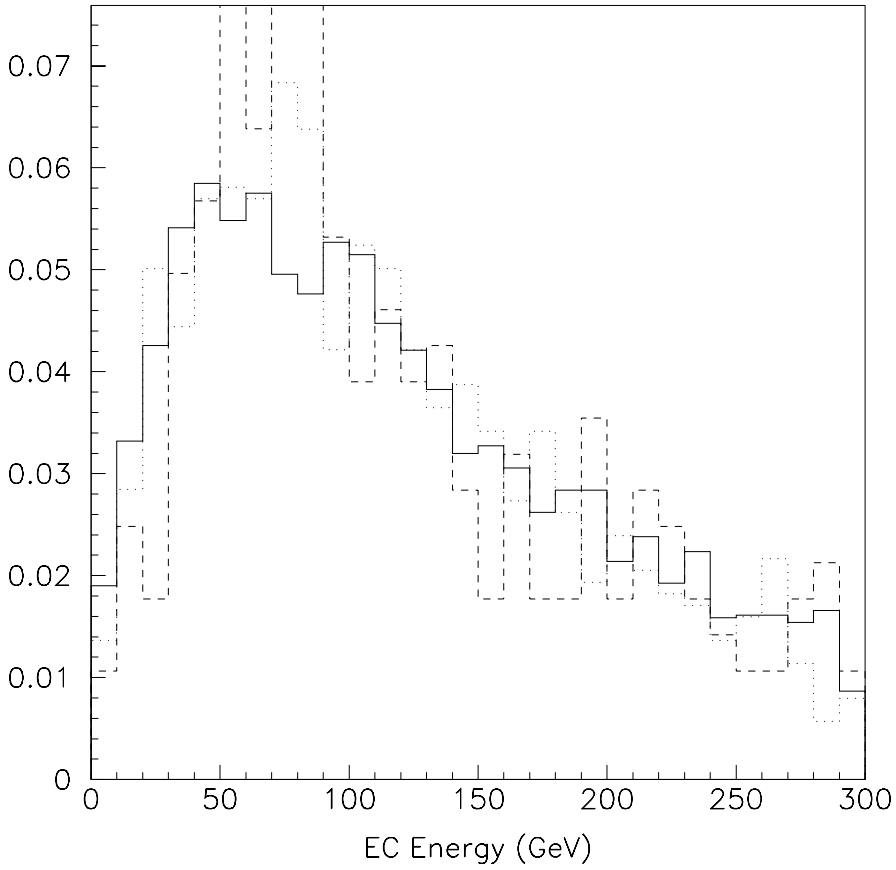

Figure 7: The distribution of energy deposited in the north DØ end cap calorimeter ($\eta > 1.3$) when there are hits in both LØ arrays. The solid line is the data, the dashed line is from the DTUJET hard core inelastic sample and the dotted curve is the MBR sample.

Inelastic Process	Average Multiplicity		Average Energy (GeV)		LØ Acceptance (%)
	Monte Carlo	Data	Monte Carlo	Data	
Single Diffractive	7.0	7.5	68	65	9.7±0.9
Double Diffractive	6.8	—	51	—	74.7±1.6
Hard Core Inelastic	10.6	11.6	137	149	99.0±0.7

Table 5: Level Ø Acceptance for each process using DTUJET.

Inelastic Process	Average Multiplicity		Average Energy (GeV)		LØ Acceptance (%)
	Monte Carlo	Data	Monte Carlo	Data	
Single Diffractive	7.0	7.5	56	65	20.5±1.3
Double Diffractive	7.7	—	71	—	68.5±1.5
Hard Core Inelastic	10.5	11.6	136	149	95.2±0.7

Table 6: Level Ø Acceptance for each process using MBR.

Inelastic Process	Mean (%)	Stat Error (%)	Sys Error (%)
SD Acceptance ($\epsilon_{\rm SD}$)	15.1	0.8	5.4
DD Acceptance ($\epsilon_{\rm DD}$)	71.6	1.1	3.1
HC Acceptance ($\epsilon_{\rm HC}$)	97.1	0.5	1.9

Table 7: Results of the Monte Carlo LØ acceptances.

	Mean	Error
Inelastic Cross Section ($\sigma_{\rm Inelastic}$)	58.94 mb	2.19 mb
SD Cross Section ($\sigma_{\rm SD}$)	9.54 mb	0.43 mb
DD Cross Section ($\sigma_{\rm DD}$)	1.15 mb	0.17 mb
HC Cross Section ($\sigma_{\rm HC}$)	48.25 mb	2.23 mb

Table 8: Cross Sections used in the $\sigma_{\rm L\emptyset}$ calculation.

	Mean	Error
$\epsilon_{\rm SD}\sigma_{\rm SD}$	1.44 mb	0.53 mb
$\epsilon_{\rm DD}\sigma_{\rm DD}$	0.82 mb	0.094 mb
$\epsilon_{\rm HC}\sigma_{\rm HC}$	46.85 mb	2.39 mb
$(\epsilon_{\rm SD}\sigma_{\rm SD}+\epsilon_{\rm DD}\sigma_{\rm DD}+\epsilon_{\rm HC}\sigma_{\rm HC})$	49.11 mb	2.45 mb
$\epsilon_{\rm L\emptyset}$	0.95	0.02
$\sigma_{\rm L\emptyset}$	46.7 mb	2.5 mb

Table 9: Results of the calculation of $\sigma_{\rm L\emptyset}$.

7 Determination of the Luminosity Monitor Constant

The calculation of $\sigma_{\rm L\emptyset}$ is given by Equation 7.

$$\sigma_{\rm L\emptyset} = \epsilon_{\rm L\emptyset}(\epsilon_{\rm SD}\sigma_{\rm SD} + \epsilon_{\rm DD}\sigma_{\rm DD} + \epsilon_{\rm HC}\sigma_{\rm HC}) \tag{7}$$

The calculation of $\sigma_{\rm L\emptyset}$ uses the values in Tables 7 and 8. The results are shown in Table 9.

8 Conclusions

For the 1992-1993 Fermilab collider run, the observable cross section for the LØ counters is $\sigma_{\mathrm{L}\emptyset}$=46.7 $\pm$ 2.5mb using the world average for the total, elastic, and single diffractive cross sections and the more accurate determinations of the LØ trigger efficiency and acceptances for the inelastic processes. This is a 3.1% decrease over the previous value of 48.2 mb and hence increases the integrated luminosity of any data set determined using $\sigma_{\mathrm{L}\emptyset}$ = 48.2 mb. The error on $\sigma_{\mathrm{L}\emptyset}$ has been reduced from 12% to 5.4% based on the studies using two Monte Carlo event generators, MBR and DTUJET-93, and unbiased DØ data samples.

We thank the Fermilab Accelerator, Computing, and Research Divisions, and the support staffs at the collaborating institutions for their contributions to the success of this work. We also acknowledge the support of the U.S. Department of Energy, the U.S. National Science Foundation, the Commissariat à L'Energie Atomique in France, the Ministry for Atomic Energy and the Ministry of Science and Technology Policy in Russia, CNPq in Brazil, the Departments of Atomic Energy and Science and Education in India, Colciencias in Colombia, CONACyT in Mexico, the Ministry of Education, Research Foundation and KOSEF in Korea and the A.P. Sloan Foundation.

References

[1] S. Abachi, *et al.*, "The DØ Detector", Nucl. Inst. and Meth., **A338** (issue 2/3) 185-253 (1994).

[2] N. Amos, *et al.*, "Change to the DØ Luminosity Monitor Constant", Fermilab Tech. Memo. TM-1911 (1995).

[3] F. Abe *et al.*, "Measurement of the $\overline{p}p$ Total Cross Section at $\sqrt{s}$ = 546 and 1800 GeV", Phys. Rev. **D50** (1994) 5550.

[4] P. Aurenche, *et al.*, Phys. Rev. **D45** (1992) 92. See also, F.W. Bopp, *et al.*, Z. Phys. **C51** (1991) 99.

[5] A. Jonckheere, Proceedings of the Argonne National Laboratory Detector Simulation Workshop, August 1987. See also F. Carminati, *et al.*, "GEANT User's Guide", CERN Program Library (Dec 1991).

[6] J. Bantly, K. Epstein, J. Fowler, G.S. Gao, R. Hlustick, R.E. Lanou, F. Nang, R. Partridge, L. Wang, and H. Xu, IEEE Trans. on Nucl. Sci. **41**, 1274 (1994).

[7] N. Amos *et al.*, "Luminosity Calculations for DØ", DØ Note 2031 (1994).

[8] N. Amos *et al.*, "A Luminosity-Independent Measurement of the $\overline{p}p$ Total Cross Section at $\sqrt{s}$ =1.8 TeV", Phys. Lett. B 243, 158 (1990).

[9] F. Abe *et al.*, "Measurement of Small Angle $\overline{p}p$ Elastic Scattering at $\sqrt{s}$ = 546 and 1800 GeV", Phys. Rev. **D50** (1994) 5518.

[10] F. Abe *et al.*, "Measurement of $\overline{p}p$ Single Diffractive Dissociation at $\sqrt{s}$ = 546 and 1800 GeV", Phys. Rev. **D50** (1994) 5535.

[11] R. Rubenstein *et al.*, "Status of Fermilab E710", FERMILAB-Conf-93/216-E (1993).

[12] K. Goulianos, "Pomeron Flux Renormalization in Soft and Hard Diffraction", Rockefeller Preprint RU 95/E-06 (1995), submitted to Phys. Rev. Lett.